Advances in Engineering Materials, Structures and Systems: Innovations, Mechanics and Applications – Zingoni (Ed.)
© 2019 Taylor & Francis Group, London, ISBN 978-1-138-38696-9

A semi-analytical approach to the evaluation of the local collapse mechanisms of masonry domes subject to seismic loads

F. Foti
Department of Civil and Environmental Engineering, Politecnico di Milano, Milan, Italy

A. Manzo
Department of Architecture and Urban Studies, Politecnico di Milano, Milan, Italy

C. Chesi
Department of Architecture, Built Environment and Construction Engineering, Politecnico di Milano, Milan, Italy

ABSTRACT: In the present work, a semi-analytical approach based on the limit analysis theory is applied to unreinforced masonry domes subject to self-weight and seismic loads. Local flexural failure mechanisms are investigated and a conservative, lower bound, estimate of the maximum seismic acceleration triggering the collapse of the dome is derived. The outcomes of the proposed formulation are illustrated with reference to both semi-circular arches and hemispherical domes and compared to available theoretical results from the literature.

1 INTRODUCTION

Masonry domes are widespread structural components in the architectural heritage. Due to their symbolic meaning, masonry domes have been often built to cover sacred spaces, since the Roman phase of the original classical tradition (Mainstone 1999). A long list of failures caused by past earthquakes has highlighted the seismic vulnerability of these structures, such as in the case of several Byzantine hemispherical domes in the Mediterranean area, not existing anymore or rebuilt after their collapse, see e.g. (Manzo 2017).

Several studies have been recently devoted to the development of refined numerical strategies to investigate the seismic behavior of masonry domes, e.g. (Atamturktur & Sevim 2012). Large numerical models, however, are computationally demanding and challenging to set up for complex structural systems, such as typical historical buildings.

Simple and reliable analytical tools, hence, are still of paramount importance for the preliminary assessment of the seismic capacity of masonry domes. At the same time, analytical tools pave the way for a deeper understanding of the main geometric and mechanical parameters that control the structural behavior.

The theory of limit analysis, based on the classic Heyman's assumptions (see e.g. (Heyman 1969, Heyman 1995)), has been already successfully applied to investigate the collapse mechanisms of masonry arches under both gravitational and seismic loads, see e.g (Alexakis & Makris 2014). Applications to domes, instead, are comparatively few and typically restricted to the case of vertical loads (e.g. Oppenheim et al. (1989)).

In the present work, a semi-analytical approach based on the limit analysis theory is applied to unreinforced masonry domes subject to self-weight and seismic loads. Local flexural failure mechanisms are investigated and a conservative, lower bound, estimate of the maximum seismic acceleration triggering the collapse of the dome is derived. The outcomes of the proposed formulation are illustrated with reference to both semi-circular arches and hemispherical domes and compared to available theoretical results from the literature.

2 GEOMETRY OF THE DOME

The present work focuses on hemispherical domes made of bricks laid on horizontal mortar joints, such as those typical of the Byzantine tradition. More in detail, the structures herein analyzed are characterized by constant thickness t and a simple geometry, without lanterns or openings.

Figure 1 shows a schematic representation of the dome. The radii of the inner and outer surfaces are denoted as R_i and R_o, respectively. The average radius of the dome, then, can be simply defined as: $R = \frac{R_i+R_o}{2}$. The main geometric parameter controlling the structural response of the dome is the thickness ratio $\varepsilon = \frac{t}{R}$, which is typically in the range 0.05–0.20, with lower values related to very thin structures.

The volume of an infinitesimal portion of the dome can be evaluated as:

$$dV = r^2 \cos(\phi)\, d\theta\, d\phi\, dr \tag{1}$$

where r, θ, ϕ are the spherical coordinates depicted in Figure 1(a).

The intersection between the dome and two meridian planes, forming a dihedral angle $\Delta\theta$, defines a lune (see the shaded volume in Figure 1(a)), i.e. a "slice" of the dome. A representative wedge of the dome, then, can be defined by cutting the lune with two parallel horizontal planes, identified by the angles ϕ_j and ϕ_i. Focusing on the case depicted in Figure 1(b) and characterized by: $0 \le \phi_i \le \phi_j \le \frac{\pi}{2}$, the volume of the wedge can be evaluated, through an integration of Eq. (1) as:

$$V(\phi_i, \phi_j) = V_{lune} \cdot (\sin(\phi_j) - \sin(\phi_i)) \tag{2}$$

where V_{lune} is the total volume of the lune, i.e.: $V_{lune} = \left(1 + \frac{1}{12}\varepsilon^2\right) \Delta\theta R^2 t$.

The centroid of the wedge belongs to the plane (x, z) in Figure 1(b), and can be identified through the coordinates $X_{g,ij} = R\bar{X}_{g,ij}$ and $Z_{g,ij} = R\bar{Z}_{g,ij}$, with:

$$\bar{X}_{g,ij} = \bar{X}_{g,ij}(\phi_i, \phi_j) = \\ = \frac{1}{2} \frac{1+\frac{1}{4}\varepsilon^2}{1+\frac{1}{12}\varepsilon^2} \frac{\phi_j - \phi_i + \frac{1}{2}(\sin(2\phi_j) - \sin(2\phi_i))}{\sin(\phi_j) - \sin(\phi_i)} \tag{3}$$

$$\bar{Z}_{g,ij} = \bar{Z}_{g,ij}(\phi_i, \phi_j) = \\ = \frac{1}{2} \frac{1+\frac{1}{4}\varepsilon^2}{1+\frac{1}{12}\varepsilon^2} \frac{\sin^2(\phi_j) - \sin^2(\phi_i)}{\sin(\phi_j) - \sin(\phi_i)} \tag{4}$$

Eqs. (2)–(4) can be easily extended to deal with the more general case characterized by $0 \le \phi_i \le \phi_j \le \pi$. The results, here omitted for the sake of conciseness, are fully reported in (Manzo 2017) under the additional simplifying assumption: $\frac{1+\frac{1}{4}\varepsilon^2}{1+\frac{1}{12}\varepsilon^2} \simeq 1$.

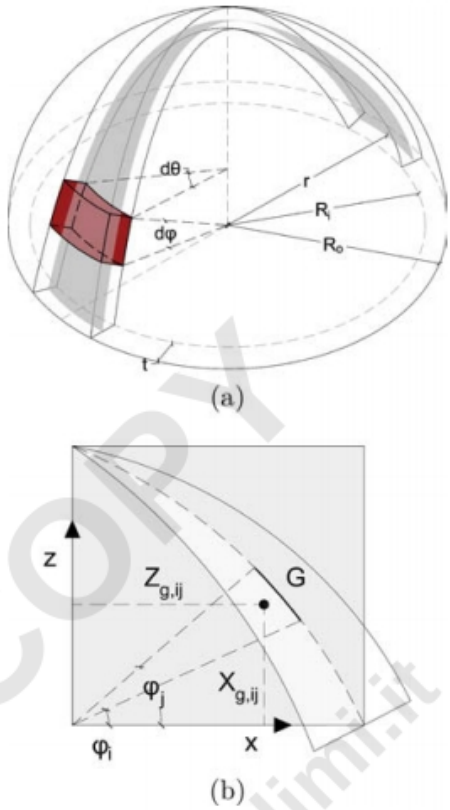

Figure 1. Schematic representation of the geometry of the hemispherical dome. (a) Definition of the spherical coordinates (r, θ, ϕ). The shaded portion of the dome corresponds to a lune related to the infinitesimal dihedral angle $d\theta$. (b) Centroid of the wedge identified by the angles ϕ_j and ϕ_i.

3 ANALYSIS OF THE LOCAL COLLAPSE MECHANISM

In this section, a simplified procedure is presented for the analysis of the local flexural failure mechanism of a hemispherical masonry dome under seismic loads. The proposed formulation relies on the classic Heyman's assumptions for the limit analysis of masonry structures (Heyman 1969, Heyman 1995):

- Masonry has no tensile strength, i.e. no tensile stress can be transferred between adjacent voussoirs. This assumption may be slightly inaccurate, since brick patterns are typically able to carry a certain amount of tensile forces due to interlocking and frictional interactions between the voussoirs (see e.g. Foraboschi (2014), Beatini et al. (2018)), but can be regarded as "safe" in the spirit of the lower bound theorem of limit analysis.
- Masonry has infinite compression strength. This assumption, which amounts to neglect collapse modes due to crushing of the material, can be supported by noticing that failure in historical vaulted structures is typically due to a loss of stability rather than lack of material compression strength (Foraboschi 2014).
- Sliding failure cannot occur, i.e. friction between the voussoirs is large enough to prevent any possible relative displacement between them. This assumption, which amounts to neglect shear failure modes, is typically satisfied in thin vaulted structures (Foraboschi 2014). Shear failure modes, however, could be relevant for thick domes (i.e. with thickness ratio greater than about 0.3). An extension of the proposed formulation including sliding failure modes is currently under development.

Starting from Heyman's assumptions, Oppenheim et al. (1989) investigated the collapse of axisymmetric domes under the action of self-weight. By recognizing the key role of meridian cracking under the action of vertical loads, Oppenheim et al. (1989) assumed zero hoop (or circumferential) stresses within the dome. A purely compressive loading path, entirely contained within the thickness of the dome and in equilibrium with the vertical external loads, was then found by the authors. The solution is characterized by compression forces acting only in the meridian direction. The approach proposed by Oppenheim et al. (1989)

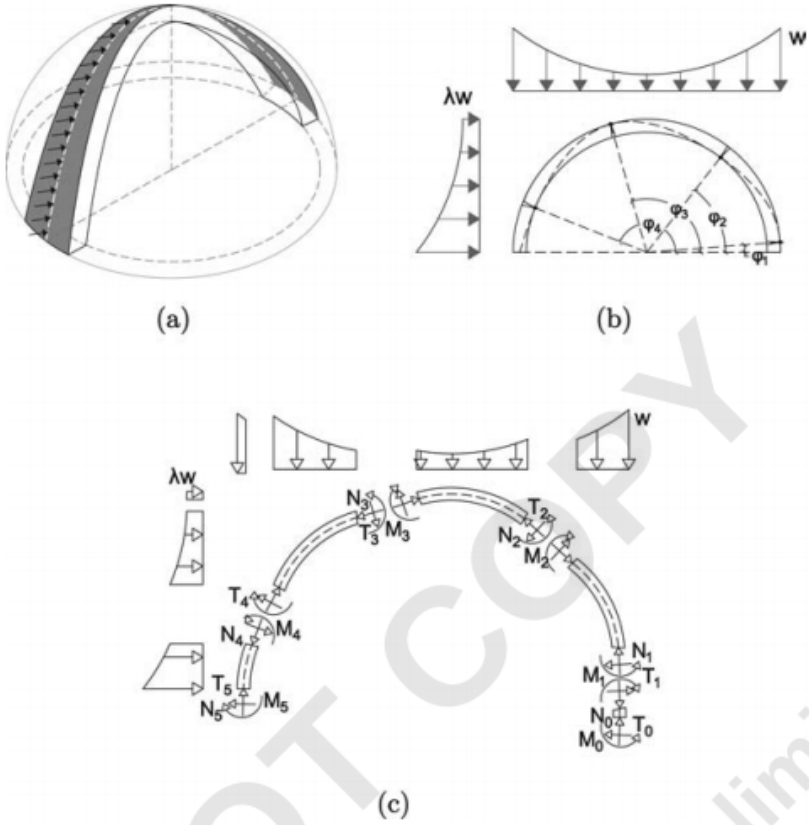

Figure 2. (a) Selection of the lune element resisting to the seismic horizontal loads. (b) Vertical section of the lune crossing its middle surface. Schematical representation of the assumed flexural failure mechanism. (c) Free body diagram highlighting the internal forces at the hinges of the mechanism and at the springing sections of the dome.

amounts to model the masonry dome as a parallel assembly of independent lunes (slices of dome, defined as in Section 2). This is a traditional modelling assumption, which can be traced back to the early works of the XVIII century on the stability of masonry domes (see e.g. Benvenuto (2010), Ottoni (2012)).

Modelling a masonry dome as an assembly of lunes can be inaccurate, since the effects of possible compressive stresses within the cap of the dome (i.e. an azimuthal portion of the dome surrounding the crown) are disregarded, but it is "safe" since it allows to define a lower bound value of the external loads triggering the collapse of the structure. The same assumption of zero hoop stresses, hence, is adopted in the present paper and extended to deal with the combined action of vertical loads due to self-weight and seismic horizontal loads.

The seismic action is assumed to be applied to a single lune of the dome, as it is schematically depicted in Figure 2. This simplifying assumption corresponds to the "worst scenario" for the evaluation of the maximum value of the horizontal loads that can be sustained by the dome. Both the effects of a possible load redistribution among adjacent lunes and the buttressing action of the rest of the dome, indeed, are neglected.

Figure 2(b) shows a vertical (centroidal) section of the lune under the action of self-weight, w, and of a simplified loading distribution representing seismic loads. The horizontal loads are linearly proportional to the self-weight and the proportionality coefficient λ can be regarded as the ratio between the seismic acceleration and the gravitational one. Being based on a somewhat conventional definition of an equivalent static loading condition, the proposed procedure doesn't allow to capture the effects of the complex dynamic response of the structure. It allows, however, for a quick preliminary assessment of the value of seismic acceleration triggering the failure of the dome.

Figure 2(b) also shows the assumed flexural failure mechanism of the lune. The dashed line is a qualitative representation of the thrust line associated to the mechanism, i.e. the geometric locus of the application points of the resultant force acting on the cross sections of the lune. Cross sections are herein conventionally defined in the radial direction, although different orientations (e.g. in the vertical direction) could also be induced by the stereotomy of the dome (see e.g. (Alexakis & Makris 2014)).

The failure mechanism is characterized by four hinges, which are identified by the angles ϕ_k ($k = 1, ..., 4$) and can be conveniently listed in the

vector: $\boldsymbol{\phi} = [\phi_1, \phi_2, \phi_3, \phi_4]^T$. The two springing sections of the lune, instead, can be formally identified by the angles: $\phi_0 = 0$ and $\phi_5 = 2\pi$. The thrust line associated to the mechanism is everywhere contained within the thickness of the lune. The thrust line touches the extrados of the lune at the hinges ϕ_1 and ϕ_3; the intrados at the hinges ϕ_2 and ϕ_4.

The four hinges naturally induce a partition of the lune in five wedges, as it is schematically depicted in Figure 2(c). Each portion of the lune must be in equilibrium under the action of all the external loads (i.e. vertical and horizontal) and of the internal forces N_k, T_k, M_k $(k = 0, ..., 5)$ acting at its end sections. The equilibrium equations of the generic portion of the lune, identified by the two angles ϕ_j and ϕ_i (with $\phi_j \geq \phi_i$), can be stated in the following non-dimensional form:

$$\bar{N}_i \cos(\phi_i) - \bar{T}_i \sin(\phi_i) - \bar{N}_j \sin(\phi_j) + \\ + \bar{T}_j \cos(\phi_j) - \bar{V}_{ij} = 0 \tag{5}$$

$$-\bar{N}_i \sin(\phi_i) - \bar{T}_i \cos(\phi_i) + \bar{N}_j \cos(\phi_j) + \\ + \bar{T}_j \sin(\phi_j) + \lambda \bar{V}_{ij} = 0 \tag{6}$$

$$\bar{N}_i - \bar{N}_j + \bar{M}_i - \bar{M}_j - \lambda \bar{V}_{ij} \bar{Z}_{g,ij} - \bar{V}_{ij} \bar{X}_{g,ij} = 0 \tag{7}$$

where: $\bar{N}_k = \frac{N_k}{\gamma V_{lune}}$, $\bar{T}_k = \frac{T_k}{\gamma V_{lune}}$, $\bar{M}_k = \frac{M_k}{\gamma V_{lune} R}$, $k = i, j$, V_{lune} is the volume of the lune (see Section 2) and γ the weight per unit of volume of the dome. Moreover $\bar{V}_{ij}$ is the non-dimensional volume of the wedge, defined as $\bar{V}_{ij} = \frac{V(\phi_i, \phi_j)}{V_{lune}}$ (see also Eq. (2)), while $\bar{X}_{g,ij}$ and $\bar{Z}_{g,ij}$ are the non-dimensional coordinates of the wedge centroid, already defined in Eqs. (3) and (4).

By imposing that the thrust line touches the intrados or extrados at the four hinge locations, the following additional conditions can also be stated:

$$\bar{M}_1 - \frac{1}{2}\varepsilon \bar{N}_1 = 0 \tag{8}$$

$$\bar{M}_2 + \frac{1}{2}\varepsilon \bar{N}_2 = 0 \tag{9}$$

$$\bar{M}_3 - \frac{1}{2}\varepsilon \bar{N}_3 = 0 \tag{10}$$

$$\bar{M}_4 + \frac{1}{2}\varepsilon \bar{N}_4 = 0 \tag{11}$$

where ε is the thickness ratio of the dome, already introduced in Section 2.

Eqs. (5)–(11) define a set of 19 independent algebraic equations in 19 unknowns, i.e. the internal forces at the four hinges, the ones at the springing sections and the horizontal load multiplier λ. The following compact matrix notation can also be introduced:

$$\boldsymbol{A}(\boldsymbol{\phi}) \cdot \boldsymbol{p} = \boldsymbol{b}(\boldsymbol{\phi}) \tag{12}$$

where $\boldsymbol{A}(\boldsymbol{\phi})$ and $\boldsymbol{b}(\boldsymbol{\phi})$ are, respectively, a matrix and a vector of coefficients, while $\boldsymbol{p}$ is the vector of the unknowns: $\boldsymbol{p} = [\bar{N}_0, \bar{T}_0, \bar{M}_0, ..., \bar{N}_5, \bar{T}_5, \bar{M}_5, \lambda]^T$.

The solution of Eq. (12) gives, for a generic position of the hinges defined by the trial vector $\boldsymbol{\phi}_{trial}$, the values of the non-dimensional internal force components in equilibrium with self-weight and horizontal loads associated to the multiplier λ. Simple equilibrium conditions, then, allow to obtain the non-dimensional axial force and bending moment distributions all along the lune, which will be denoted in the following respectively as $\bar{N} = \bar{N}(\phi; \boldsymbol{\phi}_{trial}) = \frac{N(\phi; \boldsymbol{\phi}_{trial})}{\gamma V_{lune}}$ and $\bar{M} = \bar{M}(\phi; \boldsymbol{\phi}_{trial}) = \frac{M(\phi; \boldsymbol{\phi}_{trial})}{\gamma V_{lune} R}$, with $0 \leq \phi \leq 2\pi$.

Knowledge of the functions $\bar{N}(\phi; \boldsymbol{\phi}_{trial})$ and $\bar{M}(\phi; \boldsymbol{\phi}_{trial})$ allows one to evaluate the non-dimensional eccentricity $\bar{e}(\phi; \boldsymbol{\phi}_{trial})$ of the line of thrust with respect to the centerline of the lune, i.e.:

$$\bar{e}(\phi; \boldsymbol{\phi}_{trial}) = \frac{M(\phi; \boldsymbol{\phi}_{trial})}{t\, N(\phi; \boldsymbol{\phi}_{trial})} = \frac{\bar{M}(\phi; \boldsymbol{\phi}_{trial})}{\varepsilon\, \bar{N}(\phi; \boldsymbol{\phi}_{trial})} \tag{13}$$

The line of thrust associated to the trial vector $\boldsymbol{\phi}_{trial}$ is not, in general, entirely contained within the thickness of the lune, differently than the line of thrust associated to the effective failure mechanism depicted in Figure 2(b). The following function, hence, can be introduced to give a quantitative assessment of the difference between the line of thrust associated to the trial vector $\boldsymbol{\phi}_{trial}$ and the one associated to the true failure mechanism:

$$F(\boldsymbol{\phi}_{trial}) = \int_0^{2\pi} f(\phi; \boldsymbol{\phi}_{trial}) d\phi \geq 0 \tag{14}$$

with:

$$f(\phi; \boldsymbol{\phi}_{trial}) = \\ = \begin{cases} \left(\bar{e}(\phi; \boldsymbol{\phi}_{trial}) - \frac{1}{2}\right)^2, & |\bar{e}(\phi; \boldsymbol{\phi}_{trial})| > \frac{1}{2} \\ 0, & |\bar{e}(\phi; \boldsymbol{\phi}_{trial})| \leq \frac{1}{2} \end{cases} \tag{15}$$

The location of the hinges of the failure mechanism can be easily obtained by searching for the zero of the function $F(\boldsymbol{\phi}_{trial})$ or, equivalently, by searching the vector $\boldsymbol{\phi}$ that satisfies the condition:

$$F(\boldsymbol{\phi}) = \inf_{\boldsymbol{\phi}_{trial}} \{F(\boldsymbol{\phi}_{trial})\} \tag{16}$$

In the present work, the optimization problem in Eq. (16) has been solved through a custom implementation of the well-known Differential Evolution algorithm (Storn & Price 1995) in the MATLAB© environment.

4 APPLICATIONS

As a first example, the proposed formulation is applied to investigate the collapse mechanism of a semi-circular arch, with radius R, under the combined action

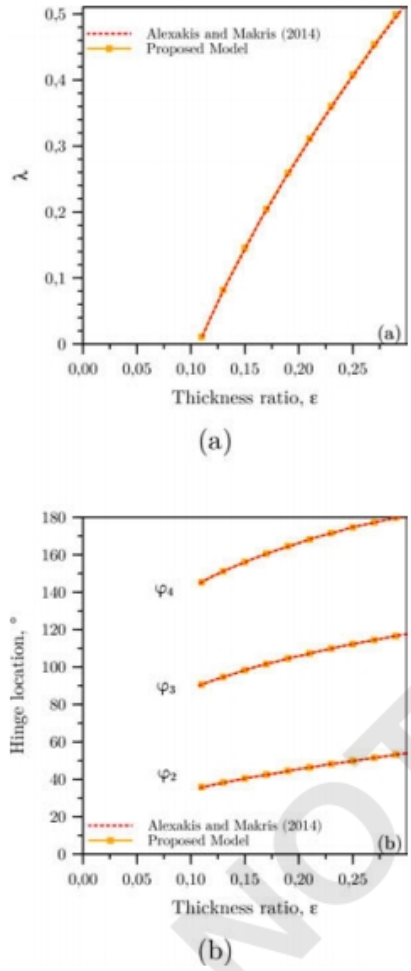

Figure 3. Semi-circular arch. Comparison between the results of the proposed formulation and the ones in (Alexakis & Makris 2014). (a) Load collapse multiplier vs. thickness ratio. (b) Location of the hinges vs. thickness ratio.

of self-weight and seismic loads. The loads are modelled according to the criteria presented in Section 3, while the relevant geometric quantities are calculated by assuming a constant thickness t. The thickness ratio of the arch is defined as $\varepsilon = \frac{t}{R}$, in analogy to the definition already introduced in the present paper for the case of hemispherical domes (see Section 2).

The outcomes of the proposed formulation are compared to the ones of the recent analytical model developed by Alexakis & Makris (2014). The model of Alexakis & Makris (2014) relies on the same basic mechanical assumptions adopted in the present work (notice that only the results in (Alexakis & Makris 2014) referred to the case of radial joints between the voussoirs will be herein considered for comparison purposes). Differently than in the present work, however, the value of the load collapse multiplier and the location of the hinges of the failure mechanism is obtained through an application of the principle of stationarity of the total potential energy.

The results are presented in Figures 3(a) and 3(b) as a function of the thickness ratio of the arch ε. Figure 3(a) shows the horizontal load collapse multiplier λ, which can also be regarded as the ratio between the seismic acceleration and the gravitational one. Figure 3(b) depicts the location of the hinges ϕ_2, ϕ_3 and ϕ_4. The position of the first hinge, not reported in the figure, is $\phi_1 = 0$ for all the values of thickness ratio herein considered.

The results of the proposed formulation are practically coincident with those of the analytical model of Alexakis & Makris (2014), showing the accuracy of the proposed semi-analytical procedure on the evaluation of both the load collapse multiplier and the location of the hinges of the flexural failure mechanism.

The formulation herein developed is then applied to investigate the flexural collapse mechanism of a hemispherical dome under self-weight and seismic loads. The results are shown in Figures 4(a) and 4(b) as a function of the thickness ratio of the dome ε.

The load collapse multiplier λ of the hemispherical dome is compared in Figure 4(a) to the one of the semi-circular arch. As expected, the hemispherical dome and the semi-circular arch cannot resist to any lateral load for values of the thickness ratio lower than about, respectively, 0.045 and 0.11. These values can be regarded as the the minimum thickness ratio of the two structures subject to self-weight only (i.e. no horizontal loads) and are in excellent agreement with the theoretical results from the literature: Heyman (1977) and Como (2016) calculated the minimum thickness ratio of the dome, respectively, as 0.042 and 0.045; Milankovitch, instead, calculated the minimum thickness ratio of the semi-circular arch as 0.1075 (see e.g. Alexakis & Makris (2014)). Figure 4(a) clearly shows that the hemispherical dome can resist to larger values of seismic acceleration (corresponding to larger values of λ) than the semi-circular arch, for values of the thickness ratio lower than about 0.22. On the contrary, for thickness ratios larger than about 0.22, the semi-circular arch performs better than the dome.

Figure 4(b) depicts the calculated location of the hinges ϕ_2, ϕ_3 and ϕ_4. The location of the first hinge, not reported in the figure, is $\phi_1 = 0$ for all the values of thickness ratio herein considered. It's worth noticing that the location of the fourth hinge of the mechanism (i.e. ϕ_4, see also Figure 2(b)) is always close to the springing section of the lune on the "windward" side of the horizontal (seismic) action. For values of the thickness ratio greater than about 0.22, however, the location of ϕ_4 actually coincides with the springing section of the lune (i.e. $\phi_4 = \pi$), leading to a "two-springing" mechanism analogous to the one that can be observed in thick semi-circular arches (see Figure 3(b)).

5 CONCLUSIONS

A simplified semi-analytical procedure has been proposed in this work for the analysis of the local flexural

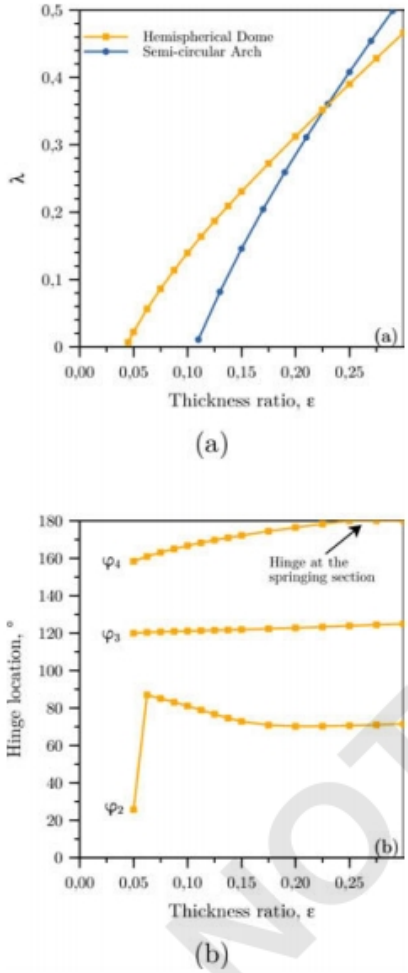

Figure 4. Hemispherical dome. (a) Load collapse multiplier vs. thickness ratio. The results for the semi-circular arch are also plotted. (b) Location of the hinges vs. thickness ratio.

failure mechanism of hemispherical masonry domes under self-weight and seismic loads.

The proposed formulation relies on the classic Heyman's assumptions for the limit analysis of masonry structures. Hoop stresses are assumed equal to zero and the dome is modelled as an assemby of independent lunes. A conservative evaluation of the maximum value of the seismic acceleration, triggering the collapse of the dome, is then obtained by assuming that the seismic action is applied to a single lune of the dome.

Being based on conventional definition of an equivalent static loading condition and on a simplified structural model, the proposed procedure doesn't allow to capture the effects of the complex dynamic response of masonry domes. It allows, however, for a quick preliminary assessment of the value of seismic acceleration triggering the failure of the dome.

ACKNOWLEDGEMENTS

The work of the first author has been partially supported by MIUR (Italian Ministry of Education, University and Research) under the project "PRIN 2015-2018 Identification and Monitoring of complex structural systems". The first author is also grateful to Prof. M.T. Di Vincenzo for all the lessons and some fruitful conversations on this paper.

REFERENCES

Alexakis, H. & N. Makris (2014). Limit equilibrium analysis and the minimum thickness of circular masonry arches to withstand lateral inertial loading. *Archive of Applied Mechanics 84*, 757–772.

Atamturktur, S. & B. Sevim (2012). Seismic performance assessment of masonry tile domes through nonlinear finite-element analysis. *Journal of Performance of Constructed Facilities (ASCE) 26*, 410–423.

Beatini et al., V. (2018). The role of frictional contact of constituent blocks on the stability of masonry domes. *Proceedings of the Royal Society A 474*, 20170740 1–21.

Benvenuto, E. (2010). *La Scienza delle Costruzioni e il suo sviluppo storico*. Edizioni di Storia e Letteratura, Roma (Italy).

Como, M. (2016). *Statica delle costruzioni storiche in muratura*. Aracne, Roma (Italy).

Foraboschi, P. (2014). Resisting system and failure modes of masonry domes. *Engineering Failure Analysis 44*, 315–337.

Heyman, J. (1969). The safety of masory arches. *International Journal of Mechanical Sciences 11*, 363–385.

Heyman, J. (1977). *Equilibrium of shell structures*. Oxford University Press, Cambridge (UK).

Heyman, J. (1995). *The stone skeleton: structural engineering of masonry architecture*. Cambridge University Press, Cambridge (USA).

Mainstone, R. (1999). *Structure in Architecture. History, Design and Innovation*. History, Design and Innovation, Ashgate, Aldershot (USA).

Manzo, A. (2017). *Santa Fosca on Torcello Island and the hypothetical dome*. Doctoral Dissertation, Politecnico di Milano, Milano (Italy).

Oppenheim et al., I. (1989). Limit state analysis of masonry domes. *Journal of Structural Engineering (ASCE) 115*, 868–882.

Ottoni, F. (2012). *Delle cupole e del loro tranello*. Aracne, Roma (Italy).

Storn, R. & K. Price (1995). *Differential Evolution - A simple and efficient adaptive scheme for global optimization over continuous spaces*. TR-95-012, International Computer Science Institute, Berkeley (USA).